Experimental interaction of magma and "dirty" coolants

C. Ian Schipper, James D.L. White, Bernd Zimanowski, Ingo Sonder, Andrea Schmid

Experimental interaction of magma and "dirty" coolants

C. Ian Schipper*[1,2], James D.L. White[2], Bernd Zimanowski[3], Ralf Büttner[3], Ingo Sonder[3], Andrea Schmid[3]

*corresponding author

Ian.Schipper@cnrs-orleans.fr

Phone: +33 (0)6 66 30 38 73

Fax: +33 (0)2 38 63 64 88

[1]Institut des Sciences de la Terre d'Orléans, CNRS - Université d'Orléans, 1A rue de la Férollerie, 45071 ORLEANS Cedex 2, France

[2]Geology Department, University of Otago, PO Box 56, Leith St., Dunedin 9016, New Zealand

[3]Physikalisch Vulkanologisches Labor, Universität Würzburg, Pleicherwall 1, 97070 Würzburg, Germany

Abstract

The presence of water at volcanic vents can have dramatic effects on fragmentation and eruption dynamics, but little is known about how the presence of particulate matter in external water will further alter eruptions. Volcanic edifices are inherently "dirty" places, where particulate matter of multiple origins and grainsizes typically abounds. We present the results of experiments designed to simulate non-explosive interactions between molten basalt and various "coolants," ranging from homogeneous suspensions of 0 to 30 mass % bentonite clay in pure water, to

heterogeneous and/or stratified suspensions including bentonite, sand, synthetic glass beads and/or naturally-sorted pumice. Four types of data are used to characterise the interactions: (1) visual/video observations; (2) grainsize and morphology of resulting particles; (3) heat-transfer data from a network of eight thermocouples; and (4) acoustic data from three force sensors. In homogeneous coolants with <~10 % bentonite, heat transfer is by convection, and the melt is efficiently fragmented into blocky particles through multiple thermal granulation events which produce associated acoustic signals. For all coolants with >~20 % sediment, heat transfer is by forced convection and conduction, and thermal granulation is less efficient, resulting in fewer blocky particles, larger grainsizes, and weaker acoustic signals. Many particles are droplet-shaped or/and "vesicular," containing bubbles filled with coolant. Both of these particle types indicate significant hydrodynamic magma-coolant mingling, and many of them are rewelded into compound particles. The addition of coarse material to heterogeneous suspensions further slows heat transfer thus reducing thermal granulation, and variable interlocking of large particles prevents efficient hydrodynamic mingling. This results primarily in rewelded melt piles and inefficient distribution of melt and heat throughout the coolant volume. Our results indicate that even modest concentrations of sediment in water will significantly limit heat transfer during non-explosive magma-water interactions. At high concentrations, the dramatic reduction in cooling efficiency and increase in mingling help to explain globular peperite, and provide information relevant to analyses of premixing associated with highly-explosive molten fuel-coolant interactions in debris-filled volcanic vents.

Keywords: peperite; granulation; magma-water interaction; experimental; fragmentation

1. Introduction

It is well established that interaction of magma with external water can have major effects on eruption dynamics (e.g., Thorarinsson et al., 1964). Styles of magma-water interaction vary from simple accelerated quenching of melt, to passive thermal granulation (Rittmann, 1962; Honnorez and Kirst, 1975; Fisher and Schmincke, 1984; Kokelaar, 1986), to intensely energetic thermohydraulic explosions (Colgate and Sigurgeirsson, 1973; Wohletz, 1983; Zimanowski et al., 1997b; Büttner and Zimanowski, 1998; Morrissey et al., 2000, Grunewald et al., 2007). Many of these processes have been observed in nature, and studied theoretically and experimentally, but most of these studies assume the "coolant" to be pure water without any sediment load. Volcanoes, in reality, are "dirty" places, where magma is far more likely to interact not with only pure water, but with mixtures of water and various particles of sedimentological and/or volcanogenic origin (White, 1991; 1996).

In very many cases of shallow magma intrusion, magma will interact with water-saturated sediments (White et al., 2000; Skilling et al., 2002; Wohletz, 2002). This will influence the cooling dynamics of intrusions where magma bodies remain intact, and will influence peperite textures in cases or regions where the magma fragments. Subaqueous lava flows may interact with pure water on their upper surfaces, but at their basal surfaces and advancing lobes they will interact with water and whatever substrate (e.g., earlier flows, volcaniclastic material, or pelagic/lacustrine sediments) over which they flow (Batiza and White, 2000; Maicher and White, 2001). At explosive vents, whether subaqueous or subaerial, processes such as juvenile particle recycling (Houghton and Smith, 1993; McClintock and White, 2006) or recapitulation (Rosseel and White, 2006; White and Houghton, 2006), and partial collapse of edifice

walls (White, 1996; Carey and Houghton, 2010) may deliver heterogeneous mixtures of particulate matter to the zone of magma ejection. These may add to pre-existing complications of surface or groundwater interacting with the magma.

Quantitative approaches to magma-water interaction are made possible by the well-constrained thermodynamic and fluid properties of both components, and a wealth of experimental data collected in multiple laboratories over the last 3 decades (e.g., Morrissey et al., 2000 and references therein). Extending these approaches to include the influence of particulate or other impurities in water is significantly more complicated. Some experiments using magma analogues have been done to address fluid mingling dynamics (Zimanowski and Büttner, 2002), heat transfer in saturated sediments (Wohletz, 2002), and the generation of peperite textures (Downey et al., 2007; 2009). Remelted magma has been used to examine the effects of dissolved salts on explosive magma-water interaction (Grunewald et al., 2007) and magma-magma fluid mingling (Zimanowski et al., 2004). There is also abundant engineering literature for quantifying processes such as heat transfer and boiling phenomena in saturated porous media (e.g., Kaviany, 1991). In the engineering case, however, the porous media themselves are often rigid, permeable networks rather than slurries or granular fluids (e.g., Haff, 1983), and industrial heat sources typically have fixed heat outputs and known, constant, geometries. Engineering approaches are thus of limited applicability to volcanic scenarios involving fluid-fluid mingling, the finite heat output of cooling magma, and even for static situations are complicated by the great potential heterogeneity and mobility of particulate matter and/or water in the substrate. As sediment is entrapped and/or mobilized, as water is vapourised and/or added to the system, as the magma supply waxes and wanes, and as magma fragments and cools, the wholesale geometry and power of the magma-water-particle system

will change to dramatic effect.

In this paper, we present the results of some very simple experiments with molten basalt, carried out to explore the very complicated scenarios of magma-water-particle interaction. We use visual observations, the morphology of particles produced, heat-transfer data, and acoustic response data, to evaluate how the non-explosive processes of hydrodynamic mingling and thermal granulation change as magma interacts with various "dirty" coolants.

2. Methods

2.1 Experimental setup

Crushed volcanic rock from Billstein/Rhön, Germany (see Section 2.2) was remelted in an open furnace containing an Al_2O_3 crucible, in order to avoid contamination of the melt. Technical details of the inductive furnace and the experimental setup can be found in Schmid et al. (2010). Figure 1 shows a picture of the system.

An insulated, cylindrical stainless steel 12 l container named the "Bismarck," was used as short time calorimeter (Fig. 1). The water used in coolants was purified before being put into the pot to ensure constant water properties for all experiments. Eight thermocouples (type K) are mounted at two vertical levels, symmetrically, to get a good measurement of the average coolant temperature during each experiment. Three Kistler® high-speed (10 Hz to 20 kHz frequency response) force sensors are mounted to the base of the Bismarck, to record the characteristic acoustic response of the interaction, and especially of fragmentation processes. An automatic stir rod was designed for experimental runs with low suspended sediment. For high-sediment coolants, the stir rod interfered with the system, and the poured melt, and was not

used. Throughout the development of the Bismarck system, experimental runs involving pure water as the coolant have been performed to calibrate and refine the experimental setup (e.g., Schmid et al., 2010). For pure water coolant, the accuracy of the thermocouples is ±0.2 ^{o}C after calibration, and the relative uncertainty in the calorimeter's heat content is 1.4 to 3.8 %. Heat loss due to imperfect insulation of the Bismarck is expected to be slightly higher for experiments involving high sediment loads, particularly in cases where melt collects as a point heat source at the base of the container. We consider this to have a negligible effect on our results, which rely on relative heat transfer styles and rates, rather than heat energy balances that require greater precision.

< Fig. 1. Bismarck >

2.2 Experimental runs

In each experimental run, 200 to 250 g of melt was poured into the coolant over 20 to 35 s.

An important physical parameter of the remelted alkalic Billstein/Rhön basalt (Zimanowski et al., 2004) used in all experiments is its rheological behaviour. The temperature dependent, non-Newtonian viscosity of the melt was determined using the method of Sonder et al. (2006), and is shown in Figure 2A. Low viscosities are required to get hydrodynamic mingling in the laboratory. Also, the low mingling energy (i.e., differential flow speed between melt and coolant) realised in the experiments and in nature means that the mingling process takes place on a time scale of seconds, necessitating a certain overheat of the melt. To satisfy these requirements, all experiments were carried out at ~1340 ^{o}C. After 3-4 hours of melting at 1340 ^{o}C some crystals may be present. Since magma is not at equilibrium during an eruption, not thermally, chemically, or thermodynamically, it is not possible to fully reconstruct

the inherently unknown physical states of all melt components. The remelting of all crystals in the Billstein melt would take at least several weeks (e.g., olivine, Thornber and Huebner, 1985). The described non-equilibrium melt represents the closest possible analogue that is practical to produce in the laboratory for these experiments. Properties of the melt and the different sediments used are given in Table 1; as are the different experimental coolant mixtures, divided into three series.

< Fig. 2. Viscosities >

< Table 1. Experimental materials and coolants >

The "dirty" coolants presented here represent single experiments that show systematic changes in interaction dynamics with sediment load throughout the experimental series.

"Series A: Homogeneous suspensions" includes four control experimental runs, designed to explore the influence of fine suspended sediment on melt interaction. A natural bentonite clay mixture (>70% montmorillonite, ~5% illite), normally used to line containment ponds, was delivered as a dry powder, and was mixed with pure water to yield different coolants, with 0%, 10%, 20%, and 30% bentonite by mass. This variation causes an increase of the coolant viscosity. At 30% bentonite content, the mixture viscosity (1 to 30 Pa s; Fig. 2B) exceeds the melt's viscosity at experimental temperature.

Clay suspensions may be thixotropic; showing reversible, time-dependent changes in viscosity depending on shear rate (e.g., Tropea et al., 2007). It can take several hours for gelling or solidification of high-concentration thixotropic mixtures to occur, depending on clay content and type. Over the time scales of our experiments and at the modest bentonite concentrations used, no manifestations of thixotropy were observed.

With time in each of the Series A coolants, there was slight settling of the sediment loads, apparent in the development of a meniscus of pure water that would develop on top of each coolant when left in a graduated cylinder. This settling/ separation occurred only after a few hours, so that the sediment was homogeneously suspended in each coolant mixture over the time scale of individual experiments. Observations made during Series A experiments are the main focus of this work.

"Series B: Heterogeneous mixtures" includes a variety of experimental runs using the coolant mixtures of Series A but with added coarse sediment; most used variable proportions of natural pumice collected from the Taupo Volcanic Zone (TVZ), New Zealand, and one used synthetic glass beads as a silicate-sand analogue (Table 1). The TVZ pumice was from an unseived but naturally sorted fall deposit (V. Manville, pers. comm., 2008) comprising pumice with a minor proportion of greywacke lithic material. Though the Series B experimental runs are here grouped together, the pumice and bead runs have different properties, especially at higher sediment loads. In the pumice mixture (Run B1), the coarse water-saturated pumice grains were strongly interlocked in a grain-supported mass, with water in interstices. The glass beads (Run B4) were neutrally buoyant in the 30% bentonite mixture, and homogeneously dispersed through the coolant volume in a non-interlocking geometry. In pumice-bearing coolants with 15 and 30% coarse sediments (B2, B4, B5), the water-saturated pumice was near-neutral- to weakly-buoyant, but dispersed in the bentonite suspension, and in the 30% bentonite mixture buoyancy effects were damped by the increased bentonite-suspension viscosity. For these mixtures the variable density of the natural clasts made some particle segregation inevitable, but it would have been quite limited because of the suspension's viscosity, particle interlocking, the small density contrasts, and because the mixtures were thoroughly stirred until some tens of

seconds before the pours began. In all Series B experiments involving pumice, significant interaction, grain-grain contact, and transient interlocking of the coarse particles was apparent, and increased with increased coarse sediment load.

"Series C: Stratified sediments" includes two experimental runs, where tight-packed pumice (C1) and tight-packed, saturated sand (C2) mixtures were placed in the bottom of the Bismarck, covering the lower four thermocouples, but not the top four. Additional clean water then covered the basal sediment layer and the top four thermocouples.

3. Results

3.1 Pour dynamics

A key aspect of the pour dynamics in all experiments was the relative ease with which the poured melt penetrated the simple or mixed coolant in the Bismarck. Because of the shallow depth of the Bismarck and reduced fragmentation of the melt when it entered mixtures versus when entering plain water, the poured melt often built up into small piles that breached the surface of the coolants. This "shoaling" was an undesired effect that occurred to some degree in all experiments (Fig. 3; Table 2). Shoaling, when accumulated basalt emerged from the upper surface of the coolants, prevented some of the poured melt in each run from interacting directly with the various coolants, and introduced substantial uncertainty to determination of the absolute amount of heat added to the system. This is particularly the case when shoaling was "transient," meaning that melt would build up to the surface and then collapse during the run, after having partially cooled to the air. Less commonly, shoaling was persistent (e.g. Fig 3D), and a rough estimate of the proportion of melt that penetrated the coolant mixture could be made by careful removal of the melt pile

that remained above the coolant surface at the end of the run. In all experimental runs, shoaling was accompanied by the production of limu o Pele bubbles (Hon et al., 1988; Clague et al., 2000; Maicher and White, 2001; Schipper and White, 2009) above the coolant surface, where melt was extended upward into a thin bubble, driven by entrapped and vapourised water. Limu was produced in all experimental runs, even those in which all melt fully penetrated the coolant, so limu fragments in the resulting particles are not solely from shoaling.

Another aspect of visual observations in each run relates to the opacity of the different coolants. In all but the clean water run (A1), observations were limited to processes occurring above the coolant surface. The observations thus included only a qualitative assessment of the ease of melt penetration and shoaling (Fig. 3), observations of any steam produced, and boiling/bubbling (Fig. 3C) of the coolants. Results from individual runs are summarized in Table 2.

< Fig. 3. Pour interaction dynamics >

< Table 2. Qualitative interaction dynamics >

3.2 Fragmentation

3.2.1 General fragmentation and particle characteristics

In this paper, the term "fragmentation" is used purely to indicate melt breakup, with no implication of explosive behaviour of any type. The extent and style of fragmentation in each experimental run can be evaluated from the proportion of poured melt that was broken up, and the types of particles formed, respectively. The degree of fragmentation ranged widely, from almost none (Fig. 4iii) when the vast majority of the poured melt simply piled up on itself, often shoaled, and solidified into a single mass, to nearly total (Fig. 4i), where virtually all the melt broke up into a variety of particles.

The particles produced in experimental runs reflect different non-explosive processes of melt break-up. Thin limu o Pele, or "bubble wall" particles are found both as individual shards from larger, broken melt bubbles (Fig. 4A, left), or are recovered as partially intact bubbles (Fig. 4A, right). Some debate surrounds whether or not naturally occurring limu o Pele is formed by explosive release of magmatic volatiles from submarine vents (e.g., Clague et al., 2008), or by entrapment and vapourisation of water (e.g., Schipper and White, 2009). Limu are common in our experiments, as well as other experiments investigating non-explosive magma-water interaction (Mastin et al., 2009), and must in these cases be produced hydromagmatically, since the experimental melt is nearly completely degassed to atmospheric pressure, and there are no explosive events. Dense, blocky and irregular glass particles (Fig. 4B) are formed by quench granulation of larger domains of melt as they are rapidly cooled, and are an important particle in the current study. Larger (> 1 cm) "vesicular" fluidal particles (Fig. 4C) are formed by hydrodynamic entrainment of domains of coolant into melt; the vesicles are not from magmatic exsolution, though some fragments have internal textures qualitatively identical to those of typical basaltic pyroclasts. Unlike vesicles in natural pyroclasts, the vesicles in the experimental particles often contain residual sediment from the coolants (Fig. 4C, right), similar to the sediment-filled vesicles that are common in natural peperites (Kokelaar, 1982; Dadd and Van Wagoner, 2002; Skilling et al., 2002 and references therein). Subspherical, dense, glass balls (Fig. 4D) are formed by hydrodynamic breakup of the melt stream in the coolant, followed by fluid reshaping before quenching (Zimanowski et al., 1991; Zimanowski and Büttner, 2003; Mastin et al., 2009). These are found variably with rough surfaces and asperities (Fig. 4D, left), or more rarely in regular shapes with smooth surfaces (Fig. 4D, right). Composite

particles (Fig. 4E) were formed in many experiments. They consist of many individual particles, dominantly of the dense blocky and glass ball types, that welded back together before solidification. These composite particles reach several cm in length, in irregular shapes, and composed of hundreds of smaller particles; others are only two or three balls fused together, often with adhering hair. In one extreme example from the 30% bentonite + 30% glass beads run (B3), a composite "grapestone" was produced entirely below the surface of the coolant (Fig. 4E, right) and was composed almost entirely of rewelded glass balls. Composite particles are inferred to represent the substructure of the melt piles visible during the runs (Fig. 4iii). They show that fragmentation took place even when there was shoaling, but that little heat was lost from the fragments prior to their almost immediate accumulation below the pour-entry point. In experimental runs that include a proportion of coarse material in the coolant mixtures, some particles are preserved with entrained sediment (not shown). Highly elongate Pele's hair particles (not shown) ranging from a few mm to >3 m long were produced in all experimental runs. Pele's hair appeared to quench instantly when it entered the coolant (only visible in clean water run A1). Though Pele's hair is often associated with explosive basaltic volcanism, these particles form whenever melt is highly, and linearly stretched before quenching (Shimozuru, 1994), and is regularly generated in experiments using basaltic melt (e.g., Mastin et al., 2009). In our experiments, some Pele's hair always forms between the crucible and Bismarck at the end of the pour, when the melt stream thins asymptotically. When such Pele's hair did not contact the coolant surface, they remained incandescent as they continued to deform for a few seconds. Pele's hair is an unavaoidable by-product of the experimental setup, and is so abundant that the fraction of Pele's hair dynamically interacting with the coolant mixtures cannot be quantified. Some glass balls have

teardrop tails (Fig. 4D, left) like those of subaerial spindle bombs, and some hair is often included in composite particles (Fig. 4E, left), strongly suggesting that some of the hair formed during fragmentation within the coolant.

< Fig. 4. Degree of granulation and particles formed >

3.2.2 Granulation in individual runs

There is a large degree of uncertainty in interpreting the grainsize data for the experimental products, due to factors such as: shoaling, pour variations, breakage of delicate particles during recovery, loss of particles while sediment was being washed away, and incomplete separation of juvenile particles from sediment (e.g., as shown by silt component in gainsize plots of Fig. 5). Complete isolation of juvenile particles from sediment in Series B experiments was impossible; however, the results from Series A experiments are more representative, and are shown in Figure 5. Even these, however, do not capture variable but noticeable amounts of very small fragments, especially flecks of limu, that were poured off during initial acquisition of the particle separates from the Bismarck.

The mean particle size produced in Series A experimental runs increases (fragmentation efficiency decreases) with increasing sediment load in the coolant.

Limu o Pele particles, and similarly, Pele's hair particles, are present through all size classes and all experiments. In all Series A experiments, limu are the only juvenile particles < 0.1-0.2 mm. Dense blocky particles dominate the size classes from ~0.2 to 3 mm in all Series A experiments, but they represent a decreasing proportion of the total particles produced as sediment load increases (red zones in Fig. 5). Larger particles (> 3 mm) in the clean water and 10% bentonite (Runs A1 and A2) are mainly dense particles that are transitional between glass lumps representing melt piles (Fig. 4iii), and compound particles (Fig. 4E). In the 20% and 30% bentonite runs (A3 and

A4), however, the larger particles are dominantly of the vesicular fluidal type (Fig. 4C), with a minor proportion of glass balls (Fig. 4D).

Particles produced in Series B experiments, except for the usual limu and hair, are mostly variable, irregular glass lumps representing melt piles with entrained sediment (Fig. 4iii). This appears to be predominantly due to the presence of the larger, variably interlocking pumice particles, which physically interfered with melt and melt-fragment dispersal. Even the smallest of glass domains collected after pumice-bearing Series B runs show that pumice was entrained into the melt. The particles produced in the 30% bentonite + 30% beads run (B3), which lacked large angular particles to obstruct melt-coolant interaction, and in which there is no grain interlocking, resulted in abundant glass balls (even though the melt entered the coolant as a continuous stream), and the characteristic "grapestone" pictured in Figure 4E (right).

< Fig. 5: Grainsize and componentry of Series A >

3.3 Time-temperature response

The average temperature increase (ΔT) recorded by the network of 8 thermocouples, calculated as $\Delta T = T_{max} - T_o$ where T_{max} is the highest average temperature recorded over time, and T_o is the average temperature just before the start of the pour, varied dramatically from run-to-run (Fig. 6A,B). In the clean water and 10% bentonite Series A runs (A1 and A2), similar ΔT of 28.6 and 29.1 °C (T_{max} of 50.2 and 51.4 °C) were recorded. For 20% bentonite run A2, a much lower ΔT of 20.6 °C (T_{max} = 40.0 °C) was recorded, and ΔT was dramatically lower still, at 8.0 °C (T_{max} = 27.7 °C), in the 30% bentonite run (A4). ΔT was very low in Series B runs, ranging from 4.5 to 7.5 °C.

The recorded ΔT values (e.g., Fig. 6A,B) are of limited value for comparing the influence of different sediment loads on heat transfer, because the shoaling effect

described above meant that different amounts of heat energy (melt mass) interacted directly with the coolants in each run. Heat transfer by bubbling and mixture ejection that followed some runs is also not captured by the thermocouples, nor is heat transferred through the base of the Bismarck, which will be more significant in cases where melt collected as a pile, or point heat-source on the base of the container. The lower absolute temperatures measured by the thermocouples during high-sediment runs also reflect the poor transmission of heat through these mixtures, which is discussed below. The time of the melt pour varied from 20 to 35 seconds in different runs, but the magnitude of this variability is insufficient to influence the relative temperature responses of the different experiments. To accommodate these inconsistencies, as well as small differences in the starting temperature of the different coolant mixtures, we normalise the temperature response in each experiment by:

$$T' = \frac{T - T_o}{T_{\max} - T_o} \qquad (1)$$

where T' is non-dimensional temperature, T_0 is initial coolant mixture temperature, and T_{max} is the maximum temperature recorded by the thermocouples. For Series A and B experiments, we use the mean temperature response from all 8 thermocouples (Fig. 6C,D), and for Series C we calculate T' separately for the two groups of four thermocouples below and above the substrate-water interface (Fig. 6H). This allows the rates and styles of heat transfer through the Bismarck volume to be compared across experimental runs, regardless of how much melt actually penetrated the coolant mixtures.

In Series A experiments (Fig. 6C), the normalised T traces of the clean water (A1) and 10% bentonite (A2) runs are nearly identical, both reaching T_{max} < 10 s after the pour. The 20% bentonite run (A3) shows a slightly delayed T'-t response, with an initially fast heat transfer, and then delayed transfer to reach T_{max}. The 30% bentonite

run (A4) is markedly different to the other Series A experiments, with a heat transfer that is comparatively gradual and very slow, with T_{max} reached only after ~15 minutes.

In addition to the fact that sediments have a lower heat capacity than water (Abu-Hamdeh, 2003), sediment of different sizes/types has different effects on heat transfer in coolants. In low water-content sediment mixtures where heat convection is inefficient, adsorption of water on charged clay particles causes stronger increases in volumetric mixture heat capacity (and thus reductions in thermal diffusivity), than are observed in mixtures where sediment in dominated by sand or larger particles (Abu-Hamdeh, 2003). Normalized Series B experimental runs (Fig. 6D) show variable heat transfer rates, the fastest in the 20% bentonite + 30% pumice run (B3), and the slowest in the 30% bentonite + 30% pumice run (B2). The influence of coarse material added to different coolants is illustrated in Figures 6E and 6F, for basic 20% and 30% bentonite coolants, respectively. In both cases, temperature response is slowed by the addition of coarse material, and for the addition of equivalent amounts of coarse (pumice) and fine (glass beads) material, the coarser material more strongly attenuates the heat transfer (Fig. 6F). The effect of varying basic coolants with equivalent proportions of coarse material (pumice) is illustrated in Fig. 6G. The addition of 30% pumice to 20% and 30% bentonite coolants slows heat transfer, but the effect is much more pronounced for the 30% bentonite coolant. This suggests that in the high water contents of our experimental coolants, addition of bentonite strongly reduces heat transfer, and further reduction of heat transfer with additional coarse sediment is less pronounced.

Normalized Series C experiments are shown in Fig. 6H. Not surprisingly, heat transfer above the sediment base is equivalent to that in the clean water run, but below

the sediment surface is equivalent to that in the pure pumice mixture run (B1). The water over sand (C2) run shows a similar response.

< Fig. 6. Temperature response >

3.4 Acoustic response

The acoustic responses as recorded by the three force transducers on the bottom of the Bismarck yield different information depending on the timescale over which their signals are viewed.

3.4.1 Long-timescale acoustic response

When viewed over the duration of the pour, the signal is dominated by the impact of the melt entering Bismarck, and by physical perturbation by any boiling of the coolant. The left panels of Figure 7 shows the acoustic response (F, mean of measurements recorded by the three sensors) as well as the mass evolution in each of the Series A runs, versus time (start of the pour is at t=0 s).

In clean water run (A1), there is a spike in the acoustic signal at the onset of melt impact, two small spikes in response in the first 10 seconds of the pour, and then a smooth, virtually noise-free response during the last 20 seconds of the pour (Fig. 7A). Qualitatively, this run was accompanied by audible cracking sounds, whereas pours into high-sediment mixtures were quiet. This pour produced a slow and steady rise, with one small perturbation, on the mass-time plot; the largest force pulses do not appear to correspond to mass-addition perturbations, but the video reveals splashes accompanying pulses in melt delivery that match roughly with the force pulses. In the final ~20 s of the pour (before maximum mass is reached), the acoustic signal is relatively smooth even though melt was still being poured, although at a waning rate.

The 10% bentonite run (A2) has an extremely noisy signal, with many spikes in acoustic signal and the mass curve throughout the ~30 seconds of the pour (Fig. 7B),

with the large spikes in the first 10 seconds each corresponding to splashing at arrival of a pulse of melt. A short shoaling episode matches the reduction in signal from 7-9 seconds. Later during the run, shoaling melt repeatedly interfered with the automatic stir rod (see Fig. 1), which hit the side of the Bismarck several times; this both induced a lot of general noise, and created spikes in the mass-time curve when the stirrer was most strongly obstructed.

The 20% bentonite (run A3, Fig. 7C) and the 30% bentonite (run A4, Fig. 7D) runs have mass-time curves that are relatively steady and free of perturbations, with periods of maximum pour rate coinciding with the periods of maximum signal. For several tens of seconds after the pour completion in each of the runs, however, there is continued acoustic noise, greater in the 30% coolant (Fig. 7D) than in the 20% (Fig. 7C). This coincides with the time the coolant was seen to boil and bubble in video of both of these runs, and the boiling was more violent in the 30% run, which is reflected in the stronger acoustic response.

The acoustic responses in Series B and C experiments (not shown) all showed spikes coincident with pour initiation, and then rapidly attenuated signals with time, and pervasive noise (as in Fig. 7C,D) coincident with the periods of boiling after the pours.

3.4.2 Short-timescale acoustic response

Granulation events involve the brittle mechanical breakage of melt, and consequently generate acoustic signals. Since multiple breakage events occur simultaneously, only the first event can be uniquely identified on the readings of each force sensor. A force signal typically starts with a relatively “low frequency” segment (in the range of several hundred Hz), followed by high frequency crackling noise. The onset of the low frequency signal is interpreted to represent the plunge of the melt jet

onto the coolant's surface, and is used as the origin of the force signal time axis (t=0). The high frequency signals are interpreted to result from thermal granulation events, and can be distinguished from other processes such as vapour film collapses, since the latter occur over longer time scales. This was verified by performing similar experiments where melt was poured into a transparent coolant tank, and recorded with a high-speed NAC® video camera at 2000 frames per second.

Figure 7 (right panels) shows the signal recorded by each force sensor in Series A experiments, with granulation marked by the onset of sinusoidal responses. The granulation signal starts at slightly different times for the three sensors (marked t_1, t_2, t_3 in Fig. 7), reflecting the time it takes for the acoustic signal to reach each sensor, depending on the proximity of the granulation locus to each.

Clean water run (A1) shows a distinct first granulation at ~0.001 s. At times longer than 0.001 s, all sensors show continued sinusoidal patterns indicating a succession of granulation events. The 10% bentonite run (A2) shows variable response, with no distinct granulation signal recorded by sensor #1. This is an enigmatic response, contradictory to the observation that the products of thermal granulation were abundant in the particles resulting from this particular run (Fig. 7B, left). All force sensors in the 20% bentonite run (A3) show strong granulation signals. The lag time between the different sensors is longer than in the clean water run (A1), possibly reflecting the slower speed of sound in multicomponent, sediment-rich coolants (Kieffer, 1977; Valentine and Wohletz, 1989). In the 30% bentonite run (A4), there is an initial granulation event recorded by sensors #2 and #3, but poorly recorded by sensor #1. These initial signals are rapidly (<0.002 s) attenuated, which we interpret as representing a single granulation event, with no subsequent events after ~0.003 s. Alternatively, other signals could be small enough, or damping high

enough, to be absorbed by the coolant.

< Fig. 7. Acoustic response >

4. Interpretation

4.1 Interaction dynamics

Although the shoaling effect observed in most of the experimental runs was an undesired effect, it illustrates an important aspect of magma-dirty coolant interaction. The high viscosity of the coolants, the presence of coarse material, and the degree to which the coarse material interlocks into a framework limits the effectiveness with which the melt pour penetrated and dispersed in the coolant. These conditions will also affect magma-sediment interaction in natural settings; where high concentrations, of interlocking particulate matter will inhibit efficient magma intrusion into the substrate.

The vigorous boiling adjacent to the melt in experimental runs with > 20% sediment (Fig. 3C) indicates what has often been termed sediment “fluidization” (Kokelaar, 1982; Busby-Spera and White, 1987). True fluidization implies the independent movement of fluid through a population of near-static solid particles; i.e., vapour moving around particles that remained more or less stationary. In this case, the process observed might be better termed “liquefaction” (Zimanowski and Büttner, 2002), because the particles remain largely coupled to the interstitial fluid as steam bubbles pass through. Sediment fluidization or liquefaction, and consequent movement of pore water and/or fine sediment, is apparent in many natural peperites, preserved as disruption of original host-sediment stratigraphy, fine sediment elutriation, or piping (Kokelaar, 1982; Busby-Spera and White, 1987; Skilling et al., 2002 and references therein). The zone of liquefaction and bubbling in the experiments was in all cases limited to a region 2 to 4 cm from the melt entry point.

4.2 Particle formation I: Hydrodynamic mingling

Hydrodynamic mingling, defined as the dispersion of domains of one immiscible liquid in another, is a process by which melt can be non-explosively fragmented. The hydrodynamic breakup of melt jets in immiscible liquids has been extensively studied due to its application to industrial processes and nuclear reactor safety (e.g., Dinh et al., 1999). In experiments designed to examine whether hydrodynamic mingling can form peperites, Zimanowski and Büttner (2002) used analogue materials to demonstrate that high shear rates (i.e., high differential velocities) and low viscosity differentials between the two fluids promote mingling, and that the mingling energy required scales with the viscosity of the liquids. Hydrodynamic mingling is not theoretically dependent on heat transfer; however, the rapid cooling of magma in contact with any coolant, and the strong dependence of melt viscosity on temperature, in reality will strongly limit the time available for mingling to occur (Büttner and Zimanowski, 1998; Zimanowski and Büttner, 2002).

Four regimes of hydrodynamic mingling were observed in our experiments: (1) no mingling because melt was thermally granulated; (2) domains of coolant were entrained in excess melt; (3) domains of melt were dispersed in excess coolant; and (4) no mingling because melt built up into a continuous pile. Since the melt was poured from the same height, at approximately the same rate (i.e., velocity) in each experimental run, shear rate throughout the experiments is our controlled variable, and the different mingling dynamics observed can be related directly to the heat transfer rates and viscosities the different coolants. Mingling dynamics are also dependent on coolant density (Table 2), and in our treatment, we consider the coolants to be viscous liquids rather than particle suspensions, so that the viscosity increase of successive

coolants is a direct function of density increases. Pumice-bearing and stratified runs are not appropriate for use in our investigation of mingling, because of particle interlocking.

Melt fragmentation in coolants with 0% and 10% bentonite was dominated by thermal granulation due to high heat transfer rates (see below). Large proportions of dense blocky (Fig. 4B) and limu (Fig. 4A) particles were produced. Thermal granulation was sufficiently extensive and rapid to either preclude significant hydrodynamic mingling, or to prevent preservation of mingling-formed particles that, if formed, were subsequently granulated.

Entrainment of ambient fluid into a jetting immiscible fluid, in this case producing vesicular particles, is important in the industrial manufacture of foams, and in casting processes. Entrainment may be extensive if fluid jets are in turbulent flow regimes (Reynolds number > ~2000), which would require basalt flow velocities greatly exceeding those examined in the current study, or in the natural formation of peperites (Zimanowski and Büttner, 2002). Entrainment may also be extensive if the jetting fluid is negatively buoyant (Friedman et al., 2007), which would be a consideration if we had jetted melt up into coolants, rather than poured it in. For our experimental geometry, the most likely form of hydrodynamic mingling leading to vesicular particles is entrapment of coolant as the melt pour passed the air/coolant interface (Lorenceau and Quéré, 2004). Above a critical plunge velocity, a melt jet will entrain a film of coolant, which then becomes dispersed as isolated droplets. Vesicular particles were common in the products of experiments with ≥20% suspended sediments, which is consistent with experimental results showing that dispersed fluid (coolant) domains increase in size and number with increasing viscosity. Furthermore, reduced heat transfer rates in higher-sediment coolants both allowed time for coolant

entrainment, and limited thermal fragmentation of the resulting vesicular particles. Dispersal of melt into excess coolant to produce glass balls (Fig. 4D) can be related to the hydrodynamic breakup of liquid jets. Four flow/fragmentation mingling regimes are recognized (Bürger et al., 1995): I) Rayleigh breakup with dripping, and no jet formation; II) transitional, "first wind regime" with jet formation and breakup; III) turbulent "second wind regime" jet breakup; and IV) atomization. Only the first two regimes are appropriate for the low pour velocities investigated here. Transition between regimes is governed by the ambient Weber number (We_a; Table 2), and jet behaviour is described in terms of coherent jet length and droplet size. Produced droplets progressively increase in number and decrease in size moving from Rayleigh breakup through to atomization. By approximating the non-pumice-bearing coolants as homogeneous fluids, and neglecting both the influence of lubricating vapour films and thermal granulation, calculated We_a place all Series A runs in the Rayleigh regime, and the 30% bentonite + 30% beads run in the first wind regime (inset to Fig. 8). An apparent lack of glass ball particles in the Series A runs with ≤10 % sediment is presumed to result from extensive thermal granulation. Series A runs with ≥ 20 % sediment did produce glass balls, but not as extensively as in the higher-density, higher-viscosity 30% bentonite + 30% beads run, presumably because of longer stable jet lengths and reduced thermal granulation. This assessment neglects the significant effects of magma's viscosity and elasticity, both of which are expected to shorten stable jet lengths and promote drop formation (Goldin et al., 1969). We note, however, that with the uncertainties in pour velocities, jet diameters, and jet properties notwithstanding, this is only a qualitative assessment of the jet breakup regimes that *would be* expected if thermal granulation did not truncate purely hydrodynamic processes. It does, however, explain the relative abundance of dense glass balls

produced in the 30% bentonite + 30% beads run, in which heat transfer was comparatively slow, and thermal granulation was comparatively inefficient.

The results above, using magma and various "dirty" coolants, illustrate key controls on hydrodynamic mingling that are consistent with previous analogue-fluid experimental work into peperite-forming mingling regimes. In agreement with Zimanowski and Büttner (2002), mingling of any type only becomes possible when the viscosity of the coolant begins to approach that of the melt; and in agreement with Büttner and Zimanowski (1998), the dispersal of coolant within excess melt is favoured over the dispersal of melt in excess coolant, unless coolant viscosity is very high and heat transfer is slow, and there are few or no large framework-forming particles. In our experiments, the only run that met all these conditions was the 30% bentonite + 30% beads mixture (Run B4), where effective melt breakup, but with limited distribution away from the site of the pour (and of initial fragmentation) allowed many fragments to subsequently weld back together as the hot spheres accumulated below the pour entry point (e.g., Fig. 4F). The spectrum of mingling phenomena observed reflects that increased sediment loads result in both increased viscosity and density, and slower heat transfer, which cooperatively facilitate hydrodynamic mingling.

4.3 Particle formation II: Thermal granulation

Granulation is a fundamentally thermal process, promoted by high heat transfer rates, as well as the high thermal expansion coefficient, brittleness, and low fracture toughness of silicate melts. Consequently, granulation was the primary form of fragmentation in Series A experiments with <20 % suspended sediment, where initial heat transfer rates were very high (Fig. 6C). This produced the dominant fine, blocky

particles (Fig. 4B), and generated short-timescale acoustic signals at the Bismarck's force sensors (Fig. 7, right panels).

The efficiency and style of heat transfer through the volume of each different coolant controls whether or not strong thermal gradients develop, which in turn partly controls granulation efficiency. The nearly instantaneous temperature increase recorded at the thermocouples in experimental runs with < 20% bentonite (A1 and A2) indicate that at these low sediment concentrations, thermal convection throughout the Bismarck volume is efficient. The thermocouples, even though distributed around the outside wall of the Bismarck, record the temperature of the coolant as a whole, since heat is homogeneously distributed by convection throughout the coolant volume. As the experimental pour continues, the new melt interacts with coolant that, although increasing in absolute temperature, is still always at significantly lower temperature than the melt, and still capable of inducing thermal granulation. For coolants with higher (>20 %) sediment load, convection is no longer efficient, and large temperature gradations develop in the coolant. Qualitatively, this is most evident in the localised boiling around melt entry points (Fig. 3C). This occurred in all experiments with >20% sediment, and indicates that coolant in the proximity of the melt (and/or cooling melt piles) was > 100 ^{o}C, while the temperatures recorded at the thermocouples on the outside walls of the Bismarck never approached these temperatures (nor did temperatures in the < 20% sediment runs).

The consequence of thermal gradients in high-sediment experiments, is that only the first-arrived melt interacts directly with comparatively very cold coolant. Granulation is not precluded, as evidenced by the presence of dense blocky particles in the products of all experimental runs, and by the sinusoidal acoustic responses of the 20% (A3) and 30% (A4) bentonite runs (Fig. 7, right), but it is hindered by poor

heat distribution throughout the Bismarck, and also by poor melt dispersal in higher-viscosity coolants, or mixtures with framework-forming coarse particles. High-sediment coolants thus do induce granulation of the first-arrived melt (e.g., onset and then truncation of sinusoidal response in 30% bentonite run acoustic signal, Fig. 7D, right), but as melt is continuously added to the system, thermal granulation becomes less efficient, and eventually impossible.

5. Discussion

5.1 Summary of experimental results

The style of magma-"dirty" coolant interaction changes dramatically with the sediment load of the coolant. The three main aspects of these changes, summarized in Figure 8, are: (1) reduced heat transfer in high-sediment coolants; (2) increased viscosity in high-sediment coolants; and (3) interference/interlocking of large particles, in coolants bearing coarse sediment.

The relationship between the above factors are illustrated in Figure 8, as the ratio of $\Delta T_{max}/t_{Tmax}$ (maximum temperature / time to reach maximum temperature) versus sediment load. In the relationship $\Delta T_{max}/t_{Tmax}$, proportionality with ΔT_{max} and inverse proportionality with t_{Tmax} results in higher values for more and/or faster heat transfer, and it allows the different coolants to be assigned to regimes of convective and non-convective heat transfer. There is a strong decrease in heat-transfer rates as ~20% suspended bentonite is added to water in the coolant. By 30% suspended bentonite, the heat-transfer properties of the coolant are greatly reduced, and addition of further sediment to the coolant has little additional effect. This suggests that the 30% coolant has sufficiently high sediment content to physically suppress rapid convective removal of heat from the melt-coolant contact, thereby "insulating" the melt from

high-rate cooling and preventing extensive thermal fragmentation. This has a feedback effect because suppressed fragmentation, as well as welding ("de-fragmentation") of hydrodynamically formed fragments, both act to minimize the surface area available for heat transfer. Also shown on the figure are effects on the dynamics of melt-coolant interaction, from immediate granulation without mingling, through inclusion of coolant domains into the melt, through hydrodynamic fragmentation of the melt and its dispersal in coolant as the coolant density increases. Effects of particle interlocking, which reduce melt penetration and mingling, are indicated separately.

5.2 Application to natural settings

The experiments reported in this paper have general implications for most scenarios where extruding or intruding magma interacts directly with wet sediments. They have specific implications for the conditions of magma-water-sediment interaction that can lead to highly explosive molten fuel-coolant interactions (MFCI), and for the (often) more quiescent processes of peperite formation. The experiments cannot be directly linked to the formation of pillow lavas, the slow effusion of which involves quench rind formation around a large mass of still-molten melt. This slows heat transfer, and consequently there is typically little or no hyaloclastite (granulation products) associated with pillow lavas (Batiza and White, 2000).

Laboratory studies have shown that MFCI may proceed only following an essential, initial premixing phase (Zimanowski et al., 1997a), which establishes the magma-water interaction geometry and/or magma-coolant mixing ratio (Sheridan and Wohletz, 1981). In his discussion of the effects of impure coolants on MFCI, White (1996) noted that although sediment would promote the development of an efficient MFCI-ready premix, due to higher damping in the coolant, it would then in contrast

require a stronger trigger (in nature, likely by volcanic seismicity) to begin the explosive cycles of MFCI. Our results strongly support the previously-noted phenomenon (White, 1996) that hydrodynamic mingling (= premixing) is enhanced by the addition of ~10 to 30 % fine sediment to the coolant. Granulation in low-sediment runs was fast enough to preclude mingling resulting from lava-like advance and coolant incorporation, but slower heat transfer and matched viscosities in higher-sediment runs promoted hydrodynamic mingling, as indicated by formation of glass balls and vesicular particles. The experiments, however, were not designed to explore explosive interactions; thus no external MFCI trigger (e.g., Zimanowski et al., 1997b) was employed. The magnitude and style of trigger required to initiate MFCI in our experimental "dirty" coolants remains experimentally untested.

Peperites, rocks "formed essentially in situ by disintegration of magma intruding and mingling with unconsolidated or poorly consolidated, typically wet sediments" (White et al., 2000), can have a wide variety of textures, with juvenile components ranging generally from blocky to fluidal (Busby-Spera and White, 1987; Skilling et al., 2002; Squire and McPhie, 2002). Although the generation of some peperites likely involves a modified form of MFCI (Busby-Spera and White, 1987; Wohletz, 2002), the non-explosive experiments presented here pertain to more passive scenarios. Peperite textures are controlled by many factors (e.g., Skilling et al., 2002, and references therein), including highly temperature-dependent magma viscosity (Busby-Spera and White, 1987; Dadd and Van Wagoner, 2002), and the grain size characteristics of the host sediment (Kokelaar, 1982; Busby-Spera and White, 1987; Squire and McPhie, 2002). The only true "blocky" particles produced in the experiments are the fine, dense blocky products of thermal granulation (Fig. 4B), and are the products of high heat transfer rates. Coarse "blocky peperite" is often

attributed to the fragmentation of magma with high viscosity (cooler), which is fragmented by various mechanical stresses from adjacent interactions (Busby-Spera and White, 1987), or magma backpressure during continued eruption (Skilling et al., 2002; Squire and McPhie, 2002). The melt piles produced in Series B experiments involving coarse sediments can be considered analogous to coarse fluidal globular peperite (although preserved as unconsolidated particles, rather than preserved in-situ), and exemplify that hot, low-viscosity magma interacting with limited backpressure on coarse sediments can readily form globular peperite-style dispersed melt domains.

The most important scaling issue with our experiments pertains to the size and rate of the melt jet or stream that penetrates each coolant. In nature, this will be controlled primarily by magma discharge rate and interaction geometry. Generally speaking, melt jets with larger diameter and/or velocity will serve to increase the Weber number of the flow (caption to Table 2, inset to Fig. 8), promoting hydrodynamic fragmentation as the flow regime is pushed to higher regimes of jet breakup (Bürger et al., 1995). Furthermore, the influence of thermal granulation will be controlled by the abundance and type of sediment in the coolants, as well as the total volume of the coolant within the given (and probably complex) interaction geometries at different types of volcanic edifices. We expect that when interactions between melt and coolants occur under hydrostatic pressures, insulating vapour films will be thinner and less stable, leading to enhanced efficiency of thermal granulation processes (Zimanowski and Büttner, 2003).

6. Conclusions

This work represents the first experimental assessment of how non-explosive

magma-coolant interactions change as the coolants range from clean water to heavy particle-laden slurries. The large degree of heterogeneity that exists in the experimental coolants reflects the similar heterogeneity that exists in natural volcanic centres. Despite this heterogeneity, several key aspects of magma-"dirty" coolant interaction can be isolated:

(1) In coolants with < ~20% suspended sediment, thermal convection is efficient throughout the coolant volume. This translates to efficient melt-coolant heat transfer, resulting in extensive thermal granulation of the magma. Combined with the large viscosity difference between low-sediment coolants and magma, this significantly limits processes of hydrodynamic mingling. Resulting particles are dominantly of the dense blocky granulate type.

(2) In coolants with >~20% suspended sediment, regardless of the size of suspended particles, thermal convection is inefficient, and heat transfer throughout the coolant volume is predominantly by forced convection and/or conduction. Thermal granulation does still proceed locally, especially on first contact of magma with the coolant, but successive processes of granulation are truncated, and not self-sustained.

(3) High-sediment (>~20%) coolants containing small (clay-sand) grainsize particles promote hydrodynamic mingling, due to their increased viscosity relative to the magma with which they are interacting. This, combined with reduced heat transfer promotes mingling that progresses from coolant dispersed in melt, to melt dispersed in coolant, as sediment load increases. In high-sediment coolants that contain larger (gravel/lapilli) sized particles, the large particles hinder hydrodynamic mingling by interfering with melt trajectories.

Volcanoes are "dirty" places. The scenarios in which magma will interact with pure water are comparatively very rare compared to the scenarios in

which it will interact with water + sediment mixtures. Our results demonstrate that the style of magma-coolant interaction changes dramatically as sediment loads (and/or sediment size classes) change. Analogue experiments are essential for exploring this problem, since during real volcanic eruptions, the type of coolant(s) involved in interactions will most often be highly heterogeneous, and vary with time. As sediment types and water-sediment-magma availability changes in the course of eruption, the probability of generating highly explosive MFCI, and the style of any peperites produced will also change rapidly and dramatically in time and space.

7. Acknowledgements

Thanks to V. Manville for collecting and posting TVZ samples at short notice, to R. Murtagh for sieve analyses, and to K.R. Higbee for travel support. JDLW acknowledges support from FRST contract CO5X0804 via subcontract to GNS Science. The Würzburg group acknowledges the Deutsche Forgungsgemeinschaft (DFG), projects Zi 481/14-1 and -2.

8. References

Abu-Hamdeh, N.H., 2003. Thermal properties of soils as affected by density and water content. Biosyst. Eng., 86: 97-102. doi:10.1016/S1537-5110(03)00112-0

Batiza, R. and White, J.D.L., 2000. Submarine lavas and hyaloclastite. In: Sigurdsson, H., Houghton, B., McNutt, S.R., Rymer, H. and Stix, J. (Editors), Encyclopedia of Volcanoes. Academic Press, San Diego, pp. 361-381.

Bürger, M., Cho, S.H., Berg, E.v. and Schatz, A., 1995. Breakup of melt jets as pre-condition for premixing: Modeling and experimental verification. Nuc. Eng. Des., 155: 215-251

Busby-Spera, C.J. and White, J.D.L., 1987. Variation in peperite textures associated with differing host-sediment properties. Bull. Volcanol., 49: 765-775

Büttner, R. and Zimanowski, B., 1998. Physics of thermohydraulic explosions. Phys. Rev. E, 57: 5726-5729

Carey, R.J. and Houghton, B.F., 2010. "Inheritance": An influence on the particle size of pyroclastic deposits. Geology, 38: 347-350

Clague, D.A., Paduan, J.B. and Davis, A.S., 2008. Widespread strombolian eruptions of mid-ocean ridge basalt. J. Volcanol. Geotherm. Res., 180: 171-188. doi:10.1016/j.jvolgeores.2008.08.007.

Colgate, S.A. and Sigurgeirsson, T., 1973. Dynamic mixing of water and lava. Nature, 244: 552-555

Dadd, K.A. and Van Wagoner, N.A., 2002. Magma composition and viscosity as controls on peperite texture: an example from Passamaquoddy Bay, southeastern Canada. J. Volcanol. Geotherm. Res., 114: 63-80

Dinh, T.N., Bui, V.A., Nourgaliev, R.R., Green, J.A. and Sehgal, B.R., 1999. Experimental and analytical studies of melt jet-coolant interactions: a synthesis. Nuc. Eng. Des. 189: 299-327

Downey, W.S., Spieler, O., Kunzmann, T., Mastin, L., Dingwell, D.B. and Shaw, C.J., 2007. Hydromagmatic and peperitic interactions: A new experimental approach. EOS Trans. AGU(VB24B-08)

Downey, W.S., Kueppers, U., Scheu, B., Shaw, C.S.J. and Dingwell, D.B., 2009. Experimentally produced peperitic textures. Geophys. Res. Abs. EGU: 2009-12094

Fisher, R.V. and Schmincke, H.-U., 1984. Pyroclastic Rocks. Springer, New York, 472 pp.

Friedman, P.D., Vadakoot, V.D., Meyer Jr, W.J. and Carey, S., 2007. Instability

threshold of a negatively buoyant fountain. Exp. Fluids, 42: 751-759. Doi:10.1007/s00348-007-0283-5

Goldin, M., Yerushalmi, J., Pfeffer, R. and Shinnar, R., 1969. Breakup of a laminar capillary jet of a viscoelastic fluid. J. Fluid Mech., 38: 689-711

Grunewald, U., Zimanowski, B., Büttner, R., Phillips, L.F., Heide, K. and Buechel, G., 2007. MFCI experiments on the influence of NaCl-saturated water on phreatomagmatic explosions.; Maar-diatreme volcanism and associated processes. J. Volcanol. Geotherm. Res., 159: 126-137

Haff, P.K., 1983. Grain flow as a fluid-mechanical phenomenon. J. Fluid Mech., 134: 401-430. doi:10.1017/S0022112083003419

Honnorez, J. and Kirst, P., 1975. Submarine basaltic volcanism: morphometric parameters for discriminating hyaloclastites from hyalotuffs. Bull. Volcanol., 39: 441-465

Houghton, B. and Smith, R.T., 1993. Recycling of magmatic clasts during explosive eruptions: estimating the true juvenile content of phreatomagmatic volcanic deposits. Bull. Volcanol., 55: 414-420

Kaviany, M., 1991. Principles of Heat Transfer in Porous Media. Springer-Verlag, New York, 626 pp.

Kieffer, S.W., 1977. Sound speed in liquid-gas mixtures: water-air and water-steam. J. Geophys. Res., 82(20): 2895-2904

Kokelaar, P., 1982. Fluidization of wet sediments during the emplacement and cooling of various igneous bodies. J. Geol. Soc. Lond. , 139: 21-33

Kokelaar, P., 1986. Magma-water interactions in subaqueous and emergent basaltic volcanism. Bull. Volcanol., 48: 275-289

Lorenceau, E. and Quéré, D., 2004. Air entrainment by a viscous jet plunging into a

bath. Phys. Rev. Lett., 93: 254501. Doi:10.1103/PhysRevLett.93.254501

Maicher, D. and White, J.D.L., 2001. The formation of deep-sea Limu o Pele. Bull. Volcanol., 63: 482-496

Mastin, L., Spieler, O. and Downey, W.S., 2009. An experimental study of hydromagmatic fragmentation through energetic, non-explosive magma-water mixing. J. Volcanol. Geotherm. Res., 180: 161-170

McClintock, M.K. and White, J.D.L., 2006. Large phreatomagmatic vent complex at Coombs Hills, Antarctica: Wet, explosive initiation of flood basalt volcanism in the Ferrar-Karoo LIP. Bull. Volcanol., 68: 215-239

Morrissey, M., Zimanowski, B., Wohletz, K. and Buettner, R., 2000. Phreatomagmatic fragmentation. In: Sigurdsson, H., Houghton, B., McNutt, S.R., Rymer, H. and Stix, J. (Editors), Encyclopedia of Volcanoes. Academic Press, San Diego, pp. 431-445.

Rittmann, A., 1962. Volcanoes and Their Activity. John Wiley and Sons, New York, 305 pp.

Rosseel, J.-B. and White, J.D.L., 2006. Complex bombs of phreatomagmatic eruptions: the role of agglomeration and welding in vents of the 1886 Rotomahana (Tarawera) eruption, New Zealand. J. Geophys. Res., 111(B12205). (doi)10.1029/2005JB004073.

Schipper, C.I. and White, J.D.L., 2009. No depth limit to hydrovolcanic limu o Pele: analysis of limu from Loihi Seamount, Hawaii. Bull. Volcanol., 72: 149-164. (doi)10.1007/s00445-009-0315-5.

Schmid, A., Sonder, I., Seegelken, R., Zimanowski, B., Büttner, R., Guðmundsson, M.T., and Oddsson, B., 2010. Experiments on the heat discharge at the dynamic magma-water-interface. Geophys. Res. Lett., 37: L20311.

doi:10.1029/2010GL044963

Sheridan, M.F. and Wohletz, K.H., 1981. Hydrovolcanic explosions: the systematics of water-pyroclast equilibration. Science, 212: 1387-1389

Shimozuru, D., 1994. Physical parameters governing the formation of Pele's hair and tears. Bull. Volcanol., 56: 217-219

Skilling, I.P., White, J.D.L. and McPhie, J., 2002. Peperite: a review of magma-sediment mingling. J. Volcanol. Geotherm. Res., 114: 1-17.

Sonder, I., Büttner, R., and Zimanowski, B., 2006. Non-Newtonian viscosity of basaltic magma. Geophys. Res. Lett., 33, L02303. (doi) 10.1029/2005GL024240

Squire, R.J. and McPhie, J., 2002. Characteristics and origin of peperite involving coarse-grained host sediment. J. Volcanol. Geotherm. Res., 114: 45-61

Thorarinsson, S., Einarsson, T., Sigvaldason, G.E. and Elisson, G., 1964. The submarine eruption off the Vestmann Islands, 1963-1964. Bull. Volcanol., 27: 434-445

Thornber, C.R. and Huebner, J.S., 1985. Dissolution of olivine in basaltic liquids: experimental observations and applications. Am. Mineral., 70: 934-945

Tropea, C., Yarin, A. and Foss, J.F. (Editors), 2007. Springer Handbook of Experimental Fluid Mechanics, Volume 1. Springer-Verlag, Berlin, 1557 p.

Valentine, G.A. and Wohletz, K.H., 1989. Numerical models of plinian eruption columns and pyroclastic flows. J. Geophys. Res., 94(B2): 1867-1887

White, J.D.L., 1991. Maar-diatreme phreatomagmatism at Hopi Buttes, Navajo Nation (Arizona), USA. Bull. Volcanol., 53: 239-258

White, J.D.L., 1996. Impure coolants and interaction dynamics of phreatomagmatic eruptions. J. Volcanol. Geotherm. Res., 74: 155-170

White, J.D.L., McPhie, J. and Skilling, I., 2000. Peperite: a useful genetic term. Bull.

Volcanol., 62: 65-66

White, J.D.L. and Houghton, B.F., 2006. Primary volcaniclastic rocks. Geology, 34: 677-680

Wohletz, K., 2002. Water/magma interaction: some theory and experiments on peperite formation. J. Volcanol. Geotherm. Res., 114: 19-35

Wohletz, K.H., 1983. Mechanisms of hydrovolcanic pyroclast formation: grain-size, scanning electron microscopy, and experimental studies. J. Volcanol. Geotherm. Res., 17: 31-63

Zimanowski, B., Froehlich, G. and Lorenz, V., 1991. Quantitative experiments on phreatomagmatic explosions. J. Volcanol. Geotherm. Res., 48: 341-358

Zimanowski, B., Buettner, R. and Lorenz, V., 1997a. Premixing of magma and water in MFCI experiments. Bull. Volcanol., 58: 491-495

Zimanowski, B., Büttner, R., Lorenz, V. and Haefele Hans, G., 1997b. Fragmentation of basaltic melt in the course of explosive volcanism. J. Geophys. Res., B102: 803-814

Zimanowski, B. and Büttner, R., 2002. Dynamic mingling of magma and liquefied sediments. J. Volcanol. Geotherm. Res., 114: 37-44

Zimanowski, B. and Büttner, R., 2003. Phreatomagmatic explosions in subaqueous volcanism. In: White, J.D.L., Smellie, J.L. and Clague, D.A., (Eds) Explosive subaqueous volcanism, A.G.U Monograph, 140, 51-60 pp.

Zimanowski, B., Büttner, R. and Koopmann, A., 2004. Experiments on magma mixing. Geophys. Res. Lett., 31: L09612. (doi) 10.1029/2004GL019687

Figure Captions

Fig. 1. Experimental setup. The diameter of the steel “Bismarck” container is 24 cm.

Schematic diagrams of crucible and coolant tank modified from Schmid et al. (2010).

Fig. 2. Viscosities. A: Temperature-dependent, non-Newtonian viscosity of the Billstein/Rhön melt. The blue line represents the fitted power-law (Sonder et al., 2006) based on the measured points shown as red dots. The dashed blue line shows the extrapolated viscosity at melt temperature (1340 ^{o}C). The average relative error is ~10%. B: Non-Newtonian viscosity of the 30% bentonite coolant (A4) at room temperature.

Fig. 3. Pour interaction dynamics. Video frame grabs from various experimental runs, captured at various times after pour initiation, demonstrating examples of the full range of pour dynamics produced throughout all experiments. A: Melt easily penetrating the mixture. B: Transient shoaling events. White arrow marks incandescent early-formed shoaling limu bubble that has floated out of path of poured melt. C: Steady shoaling. White dashed line marks region of visible boiling/bubbling of mixture, around incandescent melt. D: Pervasive shoal with limited mixture penetration. The majority of the melt is piled atop the sediment mixture.

Fig. 4. Degree of granulation (i-iii) and particles formed (A-E). i-iii: Photographs of bulk experimental particles, showing qualitative range of granulation efficiency. i: Run A1, complete granulation of melt. ii: Run A3, extensive granulation, but with larger compound particles and non-granulated melt. iii: Run B1, no granulation, melt is preserved as single unit. Black arrow indicates entrainment of pumice at base, white arrow indicates large limu bubble at top. A-E: Type individual particles. A: Limu o Pele fragments. Left image shows limu o Pele shard, right shows partially preserved

bubble, at much smaller scale than in iii. B: Dense, blocky glass particles. C: Vesicular particles. White arrow in right image indicates sediment within vesicle. D: Sub-spherical, dense, individual glass balls. Note roughness, "tails," and asperities on particles in left image. E: Compound particles formed by welding of various smaller particles. Note larger scale compared to other individual particles. "Grapestone" particle in right image is almost exclusively composed of dense glass balls.

Fig. 5. Grainsize and componentry of Series A experimental runs. Grainsize increases with increasing bentonite content of coolant, and small-diameter particles in Runs A2-A4 are sediment particles that were not completely separated from juvenile particles. Componentry shown as dominant particle type (see Fig. 4) across size bins, with red background highlighting range of sizes dominated by dense blocky products of thermal granulation.

Fig. 6. Temperature response. Panels A-D show basic results. A: Temperature of mixture as average recorded by all 8 thermocouples (T_{avg}) vs. time (t) for Series A experiments. B: Normalized temperature (T'; see text for description) versus time (s) for Series A experiments. C: T_{avg} versus t for Series B. D: T' versus t for Series B, including run A2 (20% bentonite) for comparison. Panels E-H show T' versus t grouped for various mixtures. E: Constant 20% bentonite coolant, and variable coarse (pumice) contents. F: Constant 30% bentonite coolant, with variable coarse (pumice +/- glass bead) contents. G: Constant coarse content (30% pumice), with variable coolant bentonite content. H: Stratified sediments, showing average response of thermocouples from over, and under the basal coarse layer. All melt pours lasted between 20 and 35 seconds.

Fig. 7. Acoustic responses for Series A experimental runs. Left panels shows time-normalized acoustic response (F, in volts (V)) as average response from three sensors, and melt added (Δm) versus t. The main contribution to acoustic response in each is due to impact of melt being poured into the Bismarck. Grey arrows in top left panel indicate what we refer to as mass addition perturbations. Right panels show the response from each individual sensor over the first 0.01 s of interaction. The onset of a sinusoidal trace marks the first granulation event recorded at slightly different times (t_{F1}, t_{F2}, t_{F3}) depending on the relative proximity of each sensor to the locus of granulation.

Fig. 8. Summary diagram relating fragmentation processes to coolant properties. Heat transfer, expressed as the ratio $\Delta T_{max}/t_{Tmax}$ (see text for description) is the primary control on thermal granulation efficiency, detailed qualitatively in vertical greyscale bar. Total sediment is taken as a proxy for coolant viscosity, and is the primary control on hydrodynamic mingling, detailed qualitatively in horizontal greyscale bar. Note that hydrodynamic mingling is significantly limited by the presence of large particles in pumice-bearing Series B experiments, which tend to interlock. The style of fragmentation (≈ type of particles formed) in reality represents a balance between heat transfer and coolant viscosity (e.g., melt dispersal in coolant is made possible both by high coolant viscosity *and* reduced heat transfer). Dominant particle types produced are given along the curve. Inset are cartoons of the Bismarck, with schematic temperature profile (white dashed line) from melt pour to thermocouples. Note that the profile is flat in low-sediment, high $\Delta T_{max}/t_{Tmax}$, convective regime. Inset graph represents non-dimensional jet breakup length versus ambient Weber number

(We_a, Table 2), illustrating the theoretical hydrodynamic breakup regimes in the absence of thermal granulation. Note that all Series A experiments (circles) are in field I, but the 30% bentonite + 30% beads run (B4; grey diamond) is in regime II.

Tables

Table 1. Experimental materials and coolants

Melt composition	(XRF; wt.%)
SiO_2	45.31
TiO_2	2.16
Al_2O_3	12.86
FeO	11.93
MnO	0.17
MgO	10.90
CaO	10.50
Na_2O	3.14
K_2O	1.38
P_2O_5	0.54
Total	98.89
Sediment granulometry	
	Φ ($-\log_2$[mm])
bentonite*	< 2.5†
pumice	0.0 - -4.0
beads	2.5 - 1.5
sand	2.0 - 0.5

Major element geochemistry (Zimanowski et al., 2004) by X-ray fluorescence spectroscopy (XRF). *Deponit Ca-N (calcium bentonite). †The maximum grainsize of 2.5 Φ represents a small (< 25% by mass) silt content in the dominantly montmorillonite (~0.16 μm diameter particles) bentonite clay mixture.

Table 2. Qualitative interaction dynamics

Melt

No.	Description	Penetration	Shoaling	Steam	Coolant Boiling	ρ_a (kg m^{-3})	We_a
A1	water	unrestricted	brief, transient	negligible	none	1000	0.333
A2	10% bentonite	unrestricted	brief, transient	minor	none	1055	0.352
A3	20% bentonite	unrestricted	persistent	minor	weak around pour	1116	0.372
A4	30% bentonite	unrestricted	persistent	minor	vigorous around pour	1185	0.395
B1	pumice slurry	poor					
B2	30% bentonite + 30% pumice	unrestricted	brief, transient	significant	vigorous around pour		
B3	20% bentonite +30% pumice	unrestricted	persistent	minor	vigorous around pour		
B4	30% bentonite + 30% beads	slightly restricted	persistent	minor	weak, only after shoaling	1640	0.547
B5	30% bentonite + 15% pumice	slightly restricted	cyclical	minor	vigorous around pour		
C1	water over pumice	unrestricted into water poor into pumice	persistent	minor	none		
C2	water over sand	unrestricted into water none into sand	none	negligible	none		

Sediment content of different coolants given as mass %. Ambient Weber number calculated by $We_a = \rho_a d_j v_j / \sigma_m$ for different coolant densities (ρ_a), with fixed jet diameter (d_j=0.01 m), jet velocity (v_j=~0.1 m/s, estimated from mass-time curves in Fig. 7), and σ_m is interfacial tension (~0.30 N/m)

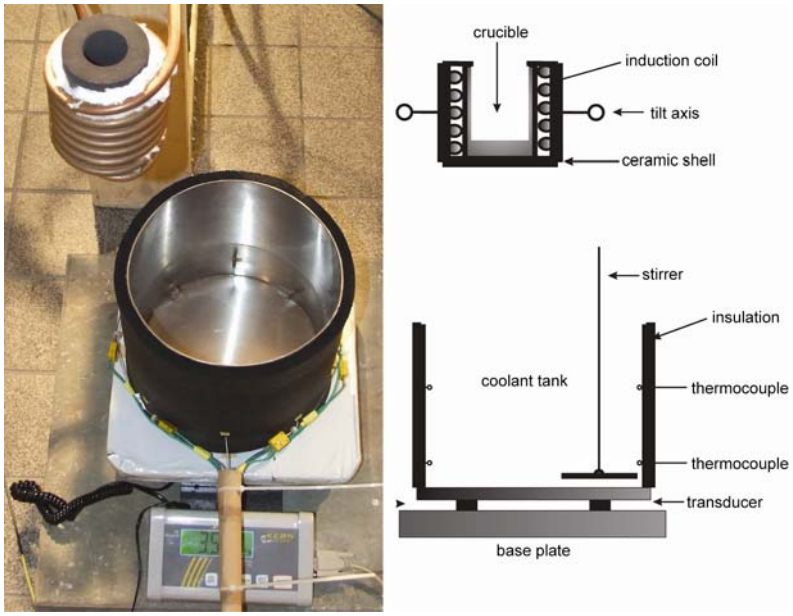
crucible
induction coil
tilt axis
ceramic shell
stirrer
insulation
coolant tank
thermocouple
thermocouple
transducer
base plate

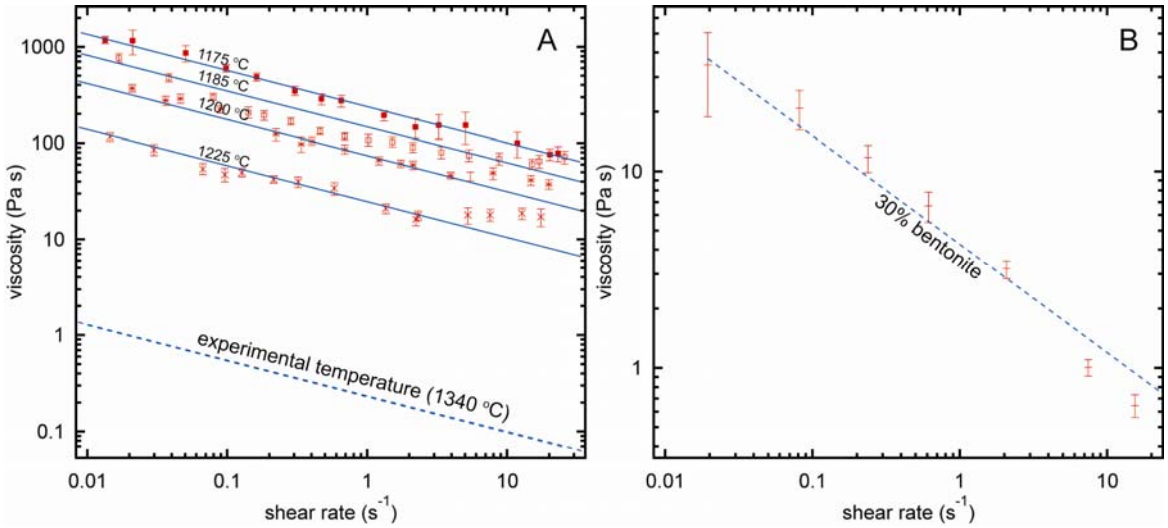
A
1175 °C
1185 °C
1200 °C
1225 °C
experimental temperature (1340 °C)
viscosity (Pa s)
shear rate (s-1)
B
30% bentonite
viscosity (Pa s)
shear rate (s-1)

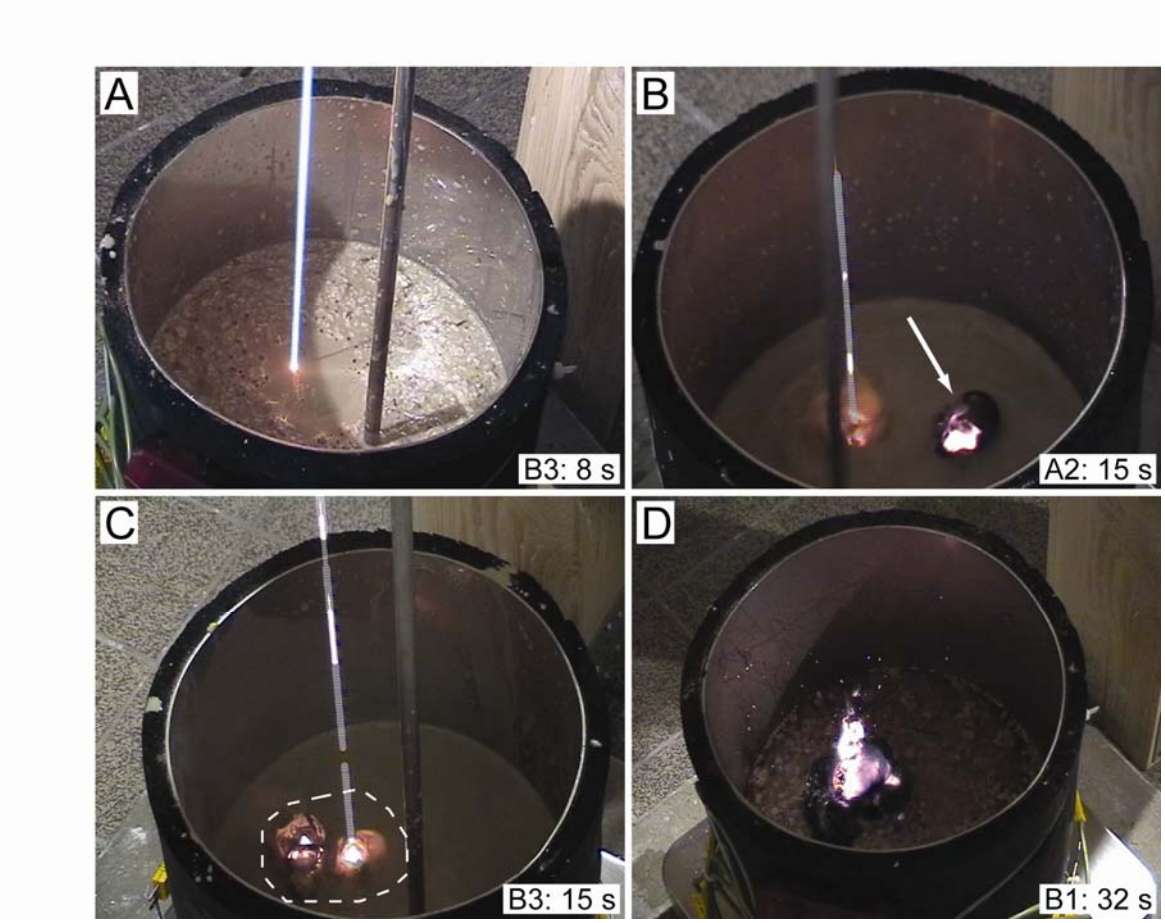
A
B3: 8 s
B
A2: 15 s
C
B3: 15 s
D
B1: 32 s

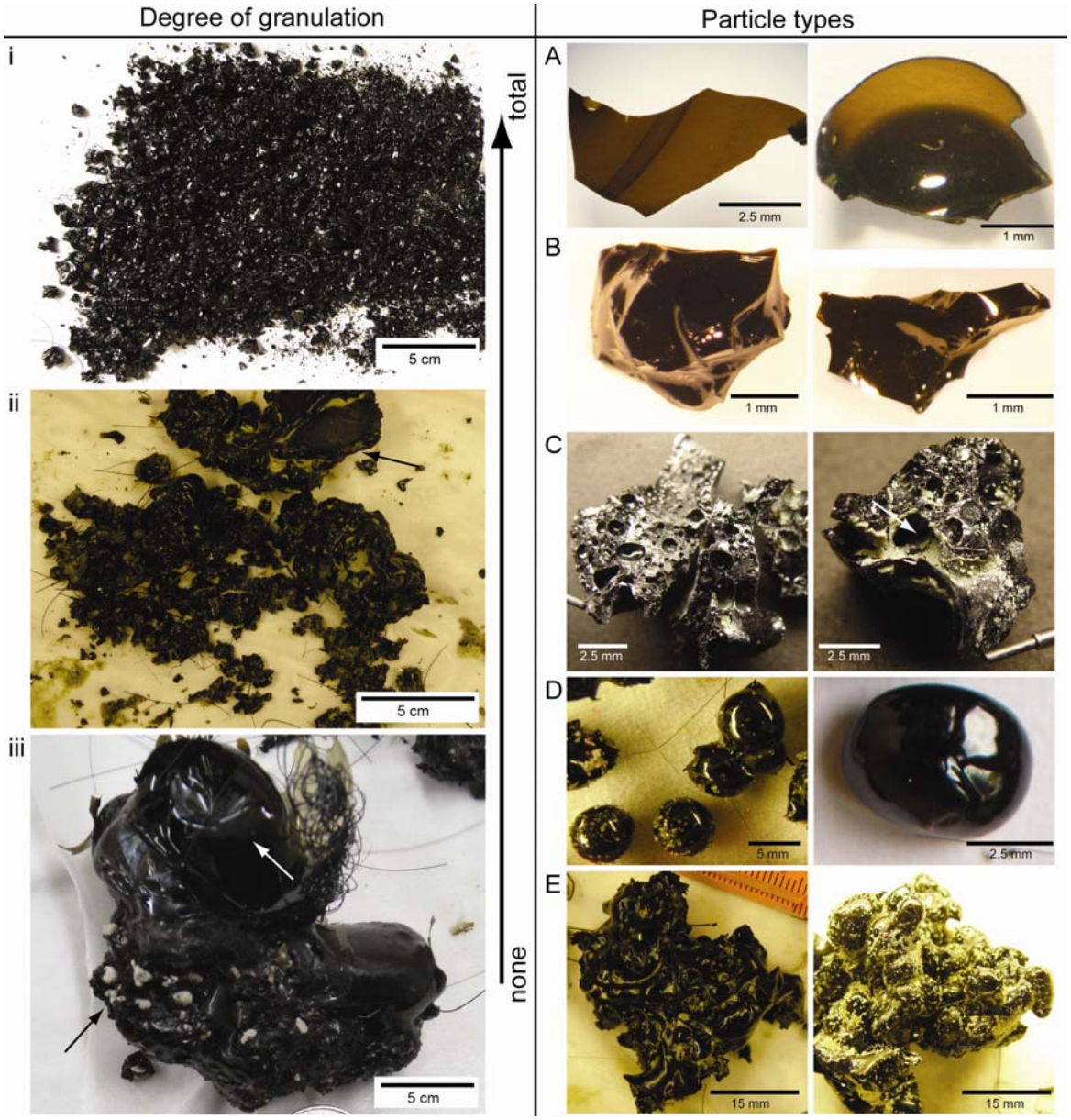
Degree of granulation
Particle types
i
ii
iii
total
none
5 cm
5 cm
5 cm
A
B
C
D
E
2.5 mm
1 mm
1 mm
1 mm
2.5 mm
2.5 mm
5 mm
2.5 mm
15 mm
15 mm

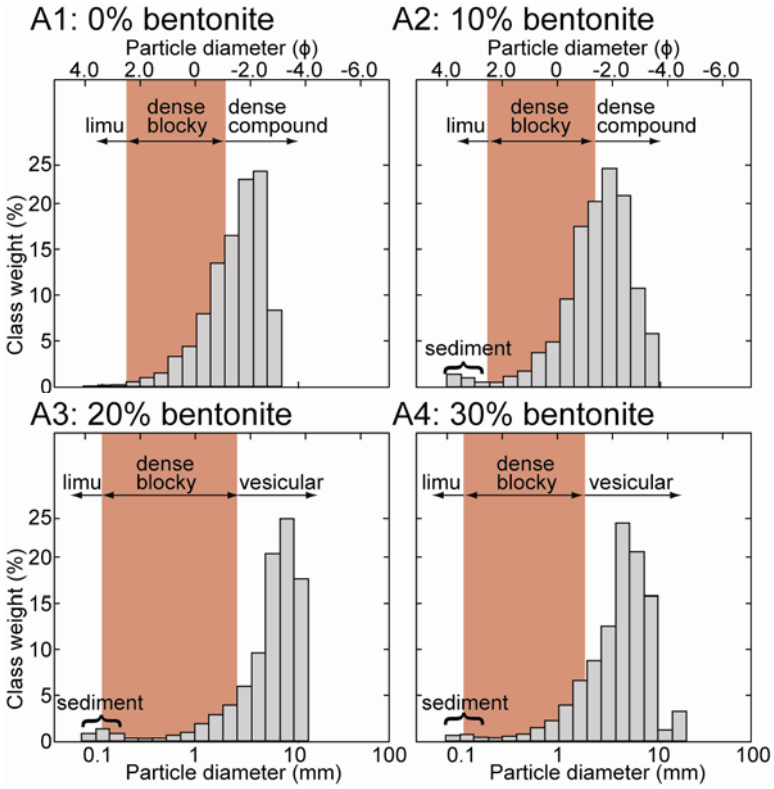
A1: 0% bentonite
A2: 10% bentonite
A3: 20% bentonite
A4: 30% bentonite
Particle diameter (ϕ)
4.0 2.0 0 -2.0 -4.0 -6.0
limu
dense blocky
dense compound
vesicular
sediment
Class weight (%)
0 5 10 15 20 25
0.1 1 10 100
Particle diameter (mm)

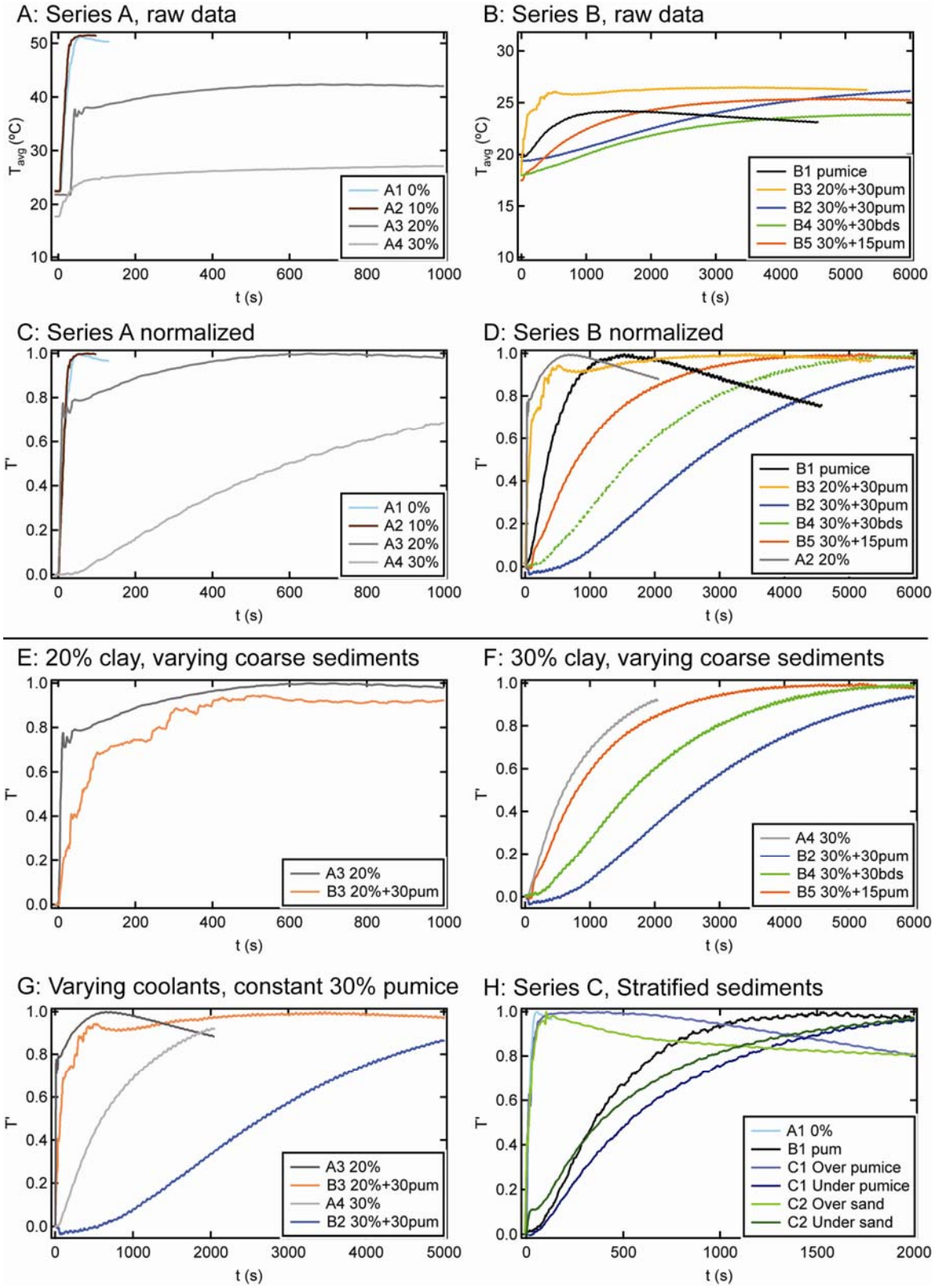
A: Series A, raw data
T_avg (°C)
t (s)
A1 0%
A2 10%
A3 20%
A4 30%
B: Series B, raw data
T_avg (°C)
t (s)
B1 pumice
B3 20%+30pum
B2 30%+30pum
B4 30%+30bds
B5 30%+15pum
C: Series A normalized
T'
t (s)
A1 0%
A2 10%
A3 20%
A4 30%
D: Series B normalized
T'
t (s)
B1 pumice
B3 20%+30pum
B2 30%+30pum
B4 30%+30bds
B5 30%+15pum
A2 20%
E: 20% clay, varying coarse sediments
T'
t (s)
A3 20%
B3 20%+30pum
F: 30% clay, varying coarse sediments
T'
t (s)
A4 30%
B2 30%+30pum
B4 30%+30bds
B5 30%+15pum
G: Varying coolants, constant 30% pumice
T'
t (s)
A3 20%
B3 20%+30pum
A4 30%
B2 30%+30pum
H: Series C, Stratified sediments
T'
t (s)
A1 0%
B1 pum
C1 Over pumice
C1 Under pumice
C2 Over sand
C2 Under sand

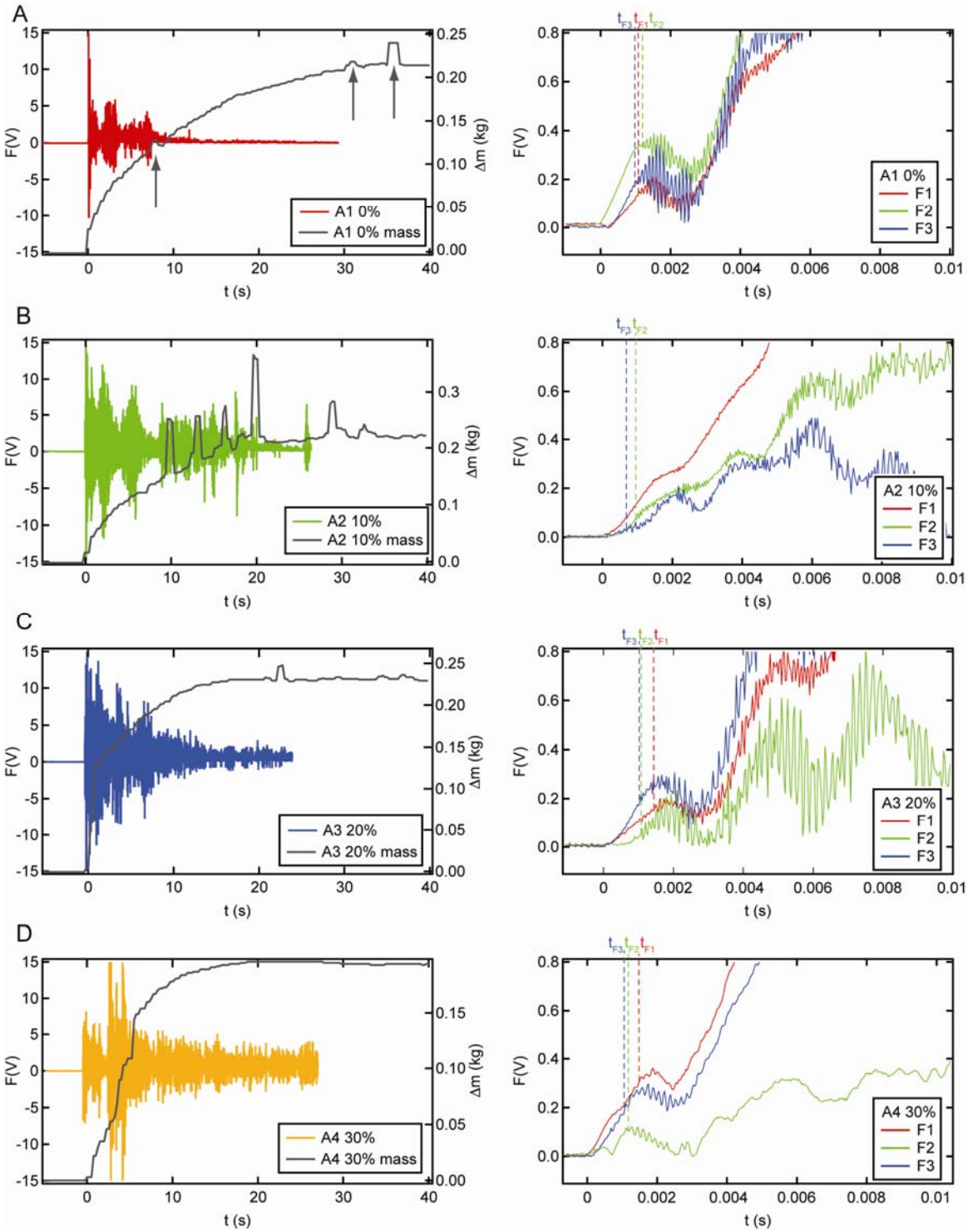
A
B
C
D
F(V)
Δm (kg)
t (s)
A1 0%
A1 0% mass
A2 10%
A2 10% mass
A3 20%
A3 20% mass
A4 30%
A4 30% mass
F1
F2
F3

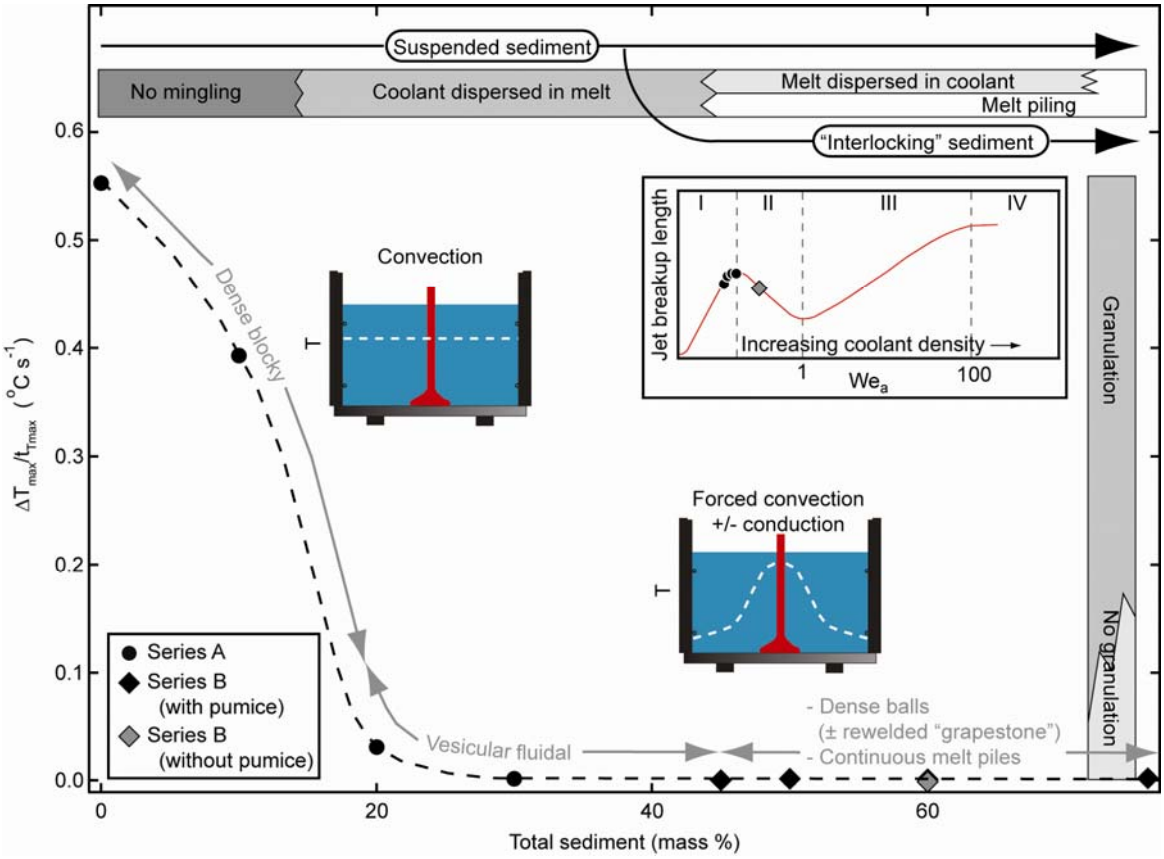
Suspended sediment
No mingling
Coolant dispersed in melt
Melt dispersed in coolant
Melt piling
"Interlocking" sediment
Convection
T
Jet breakup length
I
II
III
IV
Increasing coolant density
1
We$_a$
100
Granulation
No granulation
Forced convection
+/- conduction
T
Dense blocky
Vesicular fluidal
- Dense balls
(± rewelded "grapestone")
- Continuous melt piles
Series A
Series B
(with pumice)
Series B
(without pumice)
$\Delta T_{max}/t_{Tmax}$ ($^{o}C\ s^{-1}$)
Total sediment (mass %)
0.0
0.1
0.2
0.3
0.4
0.5
0.6
0
20
40
60